On a Dual-Sequence Stripmap Imaging Mode as Alternative for High-Resolution Wide-Swath SAR

Felipe Queiroz de Almeida, Marwan Younis, Gerhard Krieger, Alberto Moreira
German Aerospace Center (DLR), Microwaves and Radar Institute, felipe.queirozdealmeida@dlr.de
Wessling, Germany

Abstract

Future spaceborne synthetic aperture radar (SAR) systems are subject to conflicting high-resolution and wide-swath imaging requirements. As several studies show, this fundamental conflict can be resolved by advanced instrument modes employing multiple receive channels in elevation and/or azimuth (MAPS). Currently, SAR system concepts include MAPS-ScanSAR systems and Staggered-SAR systems with Scan-on-Receive (SCORE). These show disadvantages: either scalloping or increased sampling rate/on-board complexity need to be tolerated. This paper discusses a method to achieve high-resolution imaging using complementary coverage of a wide swath with two (interleaved) constant-PRI sequences, motivated by the goal of avoiding Doppler spectral gaps but also limiting system-complexity.

1 Introduction

Spaceborne Synthetic Aperture Radar (SAR) systems for remote sensing are subject to a well-known compromise between the best azimuth resolution and the maximum swath width [1]. ScanSAR [2], [3] is a well-established imaging mode in which a wide swath composed of several sub-swaths is imaged by means of alternately illuminating each sub-swath. The available illumination time is shared between a number of bursts covering different regions on the ground, trading-off azimuth resolution for wider coverage. The mode is subject to Doppler spectral gaps and thus an undesirable scalloping effect.

Multichannel architectures combined with *digital beamforming* (DBF) [4], [5], [6] show the capability of overcoming this limitation and simultaneously delivering *high-resolution wide-swath* (HRWS) SAR images. These methods can be combined with the ScanSAR imaging mode [7], currently considered an alternative for upcoming SAR systems such as HRWS [8]. One family of methods derives from the use of multiple channels in elevation [9], [10], [11], [12]. A system capable of simultaneously forming multiple elevation beams (MEB) through DBF can be used to image several sub-swaths at once, extending the SCan-On-Receive (SCORE) [13] concept. A broad transmit beam is used to illuminate all sub-swaths, whereas multiple narrow receive (Rx) beams follow simultaneously multiple radar echoes arriving from different directions. In comparison to a concept with multiple azimuth channels [14], the use of multiple elevation channels has the potential to lead to a more compact antenna design [10] and simpler signal processing.

An inherent limitation remains in the form of *blind ranges* between the sub-swaths. These are formed due to the impossibility of recording the echoes while transmitting – a characteristic of monostatic systems – and have regularly spaced positions determined by the (constant) PRF. A possible solution is Staggered SAR [15]: a fast and systematic PRI variation scheme which distributes the gaps over range and allows for narrow gaps and to be recovered by interpolation over azimuth. The mode shows the considerable advantage of a complete Doppler spectrum, but at the cost of non-uniform sampling. This drives up the average sampling rate and as a consequence the complexity, as on-board processing becomes necessary for data rate reduction.

The motivation for the dual-sequence mode, first addressed in [16], is to achieve imaging of a wide gapless swath with multiple elevation beams while keeping a uniform sampling scheme in azimuth and simultaneously avoiding Doppler gaps. It is shown that it is feasible to form images from each of the two sequences (processed independently, each with a constant PRF) and achieve a gapless wide swath by mosaicking of both. The main advantage would be to thus inherently avoid scalloping and at the same time limit the required oversampling (and thus need for on-board processing), potentially reducing system complexity.

Section 2 provides a description of the mode and the first-order design strategy. In turn, Section 3 provides a performance assessment of an exemplary planar C-Band system covering a 350 km swath. A single-channel system in azimuth, but capable of multi-beam SCORE is assumed (cf. [16] for a possible multi-channel configuration in azimuth) and the performance is compared with that in the Staggered SAR mode. Section 4 concludes the paper.

2 Mode Description

Assume two pulses sequences interleaved as shown in Figure 1. The degrees of freedom of the configuration include the pulse repetition intervals (PRIs) of the first and second sequences: PRI_1, PRI_2, respectively; and the delay Δp between their first pulses. The pulse duration τ_p is assumed to be the same for simplicity, though this is not necessary.

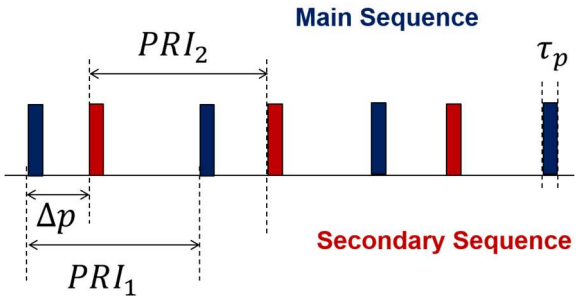

Figure 1: Schematic representation of the two pulse sequences (Main Sequence in blue and Secondary Sequence in red).

The pulses for each of the transmitted sequences are assumed to be centered at the time instants

$$t_1[n_1] = n_1 \cdot PRI_1, \quad t_2[n_2] = n_2 \cdot PRI_2 + \Delta p, \tag{1}$$

for integer n_1 and n_2.
It is assumed that the swath's echo has a duration

$$\tau_{echo} = \frac{2}{c} \cdot (R_{max} - R_{min}) + \tau_P \tag{2}$$

for slant range limits R_{min}, R_{max} such that $\tau_{echo} > \max(PRI_1, PRI_2)$, as expected in a in a multiple elevation beam system [17]. Thus, transmit events will occur during reception of the echo, leading to gaps in the acquisition for both sequences (assumed to be processed independently in azimuth, thus forming two separate images). The gaps are in this case of two distinct natures: the *co-blind* ranges (for which a sequence causes a gap on its own echo, as usual for single-sequence systems) are centered at

$$R_{11}(n_1) = \frac{c}{2} \cdot n_1 \cdot PRI_1, \quad \text{(proportional to } t_1[n_0 + n_1] - t_1[n_0]) \text{ and} \quad R_{22}(n_2) = \frac{c}{2} \cdot n_2 \cdot PRI_2; \tag{3}$$

where $n_0 = \left\lfloor \frac{2 \cdot R_{min}}{c \cdot PR_1} \right\rfloor$ is the number of travelling pulses.

And the *cross-blind* ranges (for which the other sequence causes a gap in a given sequence's echo) at

$$R_{12}(k_1, m_2) = \frac{c}{2} \cdot (\Delta p + k_1 \cdot PRI_2 - m_2 \cdot PRI_1) \quad \text{(proportional to } t_2[k_1] - t_1[m_2]); \quad R_{21}(k_2, m_1) = \frac{c}{2} \cdot (k_2 \cdot PRI_1 - \Delta p - m_1 \cdot PRI_2). \tag{4}$$

The rationale of the method is to choose the parameters such that no overlap occurs between any of these forms of gaps, i.e.

$$\begin{aligned} &|R_{11}(n_1) - R_{22}(n_2)| > \tfrac{c}{2} \cdot \tau_b \quad (a) \\ &|R_{11}(n_1) - R_{21}(k_1, m_2)| > \tfrac{c}{2} \cdot \tau_b \quad (b) \\ &|R_{12}(k_1, m_2) - R_{22}(n_2)| > \tfrac{c}{2} \cdot \tau_b \quad (c) \\ &|R_{12}(k_1, m_2) - R_{21}(k_2, m_1)| > \tfrac{c}{2} \cdot \tau_b \quad (d) \end{aligned} \tag{5}$$

where $\tau_b = \tau_p + \tau_g$ is the effective pulse length (in terms of the gap), for all relevant indices $n_1, m_1, k_1, n_2, m_2, k_2$ (i.e., leading to blind ranges R_{ij} within $[R_{min}, R_{max}]$.

If (5) is fulfilled, all regions of the swath will be covered by at least one of the two images, and thus a mosaic between them in elevation will yield a gapless acquisition. For maximum efficiency, the second sequence only needs to image the missing parts of the first image, as indicated in **Figure 2**. On the top (a), the swath as covered by the main sequence is seen, showing blind ranges caused by the first sequence itself (co-blind ranges) and the secondary sequence (cross-blind ranges). The form on the right indicates the Tx illumination. On the bottom (b), the same for the secondary sequence, illustrating the strategy of illuminating only the gaps which the first sequence is not capable of acquiring, for increased efficiency (though in practice some degree of redundant illumination is to be expected given the limitations on the directivity of the achievable elevation patterns).

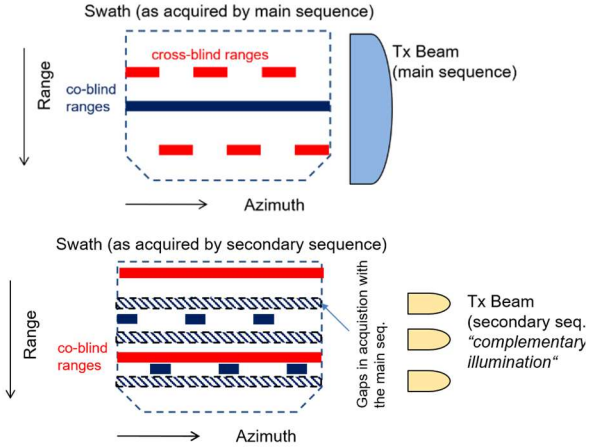

Figure 2: Swath as seen by each of the sequences, assuming the echoes of each are processed independently.

This is equivalent to mosaicking the image of a different pass of the satellite, acquired with a different PRI. This would in fact represent a simpler manner of achieving the same result, but with an obvious increase in the time for acquisition of the gapless swath. The mode can be interpreted as transmitting the sequences of the "two passes" concurrently by interleaving. This clearly comes at the cost of transmitting more pulses (with implications for number of gaps, transmitted power and range ambiguities) but a judicious choice of the parameters allows an instant acquisition of the gapless swath.

In particular, it is of interest to consider the mutually-prime integers N_1 and N_2 so that

$$N_1 \cdot PRI_1 = N_2 \cdot PRI_2. \tag{6}$$

We may assume, without loss of generality, that $N_1 < N_2 \Longrightarrow PRI_1 > PRI_2$

Defining $t_{ij} = 2/c \cdot R_{ij}$ for notational convenience, it should be noted that the conditions to be fulfilled in (5) take the form:

$$\begin{aligned} &|n \cdot PRI_1 - m \cdot PRI_2| > \tau_B && (a) \\ &|n \cdot PRI_1 - m \cdot PRI_2 + \Delta p| > \tau_B && (b), (c) \\ &|n \cdot PRI_1 - m \cdot PRI_2 + 2 \cdot \Delta p| > \tau_B && (d) \end{aligned} \tag{7}$$

for $n, m \in \mathbb{Z}$,

which explains the convenience of assumption (6), also used in [18] in a different context.

Clearly, the left-hand side of (7)(a) reaches zero, violating the condition, if $n, m = N_1, N_2$ or any integer multiple of those, i.e., at the end of each PRI cycle. This means that the *blind ranges* at multiples of the dual-PRI sequence's period $T_{12} = N_1 \cdot PRI_1 = N_2 \cdot PRI_2$ are no longer recoverable by mosaicking, but this is not a disadvantage as long as $T_{12} > 2/c \cdot (R_{max} - R_{min}) + \tau_p$. Furthermore, the remaining design variables/degrees of freedom PRI_1, N_1 and N_2 may be adapted in dependence of R_{min}, R_{max}: a favourable configuration is to match the swath extension to T_{12}, fitting the swath between two (unresolvable) blind ranges.

An important consequence of the interleaving is the increased proximity to the next pulse (of the other sequence), which tends to increase range ambiguity levels (as e.g. in a polarization-interleaved sequence used for quad-pol acquisitions). To minimize this effect, it is advisable to choose the initial delay Δp as to make the minimum distance between pulses as large as possible. The optimization can be made numerically, but it can also be shown that an optimum choice would be

$$\Delta p^* = \frac{PRI_1}{2 \cdot N_2} - \tau_B. \tag{8}$$

The result is presented here without proof for reasons of conciseness, but will be featured in a follow-up publication.

To fix ideas, assume as an example $N_1 = 2, N_2 = 3$ and the swath extension to be matched to $T_{12} = 2 \cdot PRI_1$. The delay between the sequences is chosen as $\Delta p = (PRI_1 - PRI_2)/3 = PRI_1/9$ (optimum for $\tau_B = PRI_1/18$ means a 5.5% duty cycle). The resulting gap pattern is shown in **Figure 3**. In the illustration, the position of the swath is kept fixed to illustrate how the gaps change with the pulse index. The co-blind ranges are true blind range for which all pulses are lost, but the cross-blind ranges are seen to be periodical gaps (every 2nd sample in the first sequence and every 3rd in the sequence is lost). Assuming $T_{12} > 2/c \cdot (R_{max} - R_{min}) + \tau_p$, the main sequence will image a swath with a total of $n_{gaps} = N_1 \cdot N_2 + (N_1 - 1)$ gaps, since there are N_2 cross-blind ranges for each N_1 "sub-swaths" (between pulses of the main sequence) and $N_1 - 1$ co-blind ranges.

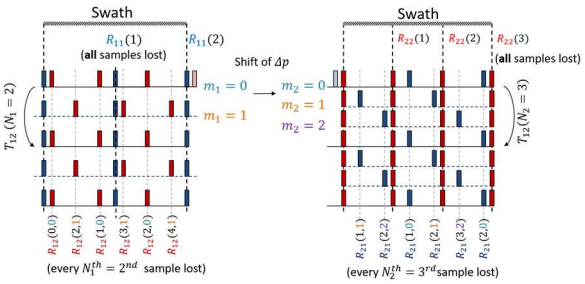

Figure 3: Gap pattern from the co-blind ranges and cross-blind ranges in the case $N_1, N_2 = 2, 3$ and $\Delta p = (PRI_1 - PRI_2)/3$ in the echoes' reference frame. In the scale of the plot, $\tau_B = PRI_1/18$.

It is interesting to note that, in general, for the *cross-blind ranges* $R_{12}(n_1, m_2)$ and $R_{21}(n_2, m_1)$ not all but rather every N_1^{th} (2nd) and N_2^{th} (3rd) samples are lost, respectively. For small N_1, N_2 as in the example, this results in severe undersampling and the gap is treated the same as a co-blind range (i.e., range bins are assumed to be discarded).

3 C-Band Design Example

This section presents simulation results to assess the SAR performance of a planar direct radiating array (DRA) system in C-Band from a Sentinel-1[19] like orbit (698 km). The system has a single channel in azimuth, but multiple elevation beams are assumed. The general parameters are described in Section 3.1. The SAR performance of the same system (in terms of the antenna and front-end parameters, kept constant as far as possible) is assessed for operation in either a Staggered SAR mode (Section 3.2) or the Dual-PRI Mode (Section 0). The Chapter is concluded with a comparison and discussion in Section 0.

3.1 Scenario and Antenna Parameters

The scenario parameters assumed for the SAR performance assessment are described in **Table 1**, whereas the antenna parameters are given in **Table 2**. The goal is to image a 350 km swath with area resolution $\delta_{2D} < 30\ \mathrm{m}^2$, total ambiguities $ASR < -23$ dB and noise sensitivity $NESZ < -22$ dB.

Platform and Swath parameters		
Orbit height	h_{orbit}	693 km
Swath width on ground	W_{ground}	350 km
Swath minimum/maximum look angle	$\theta_{min}/\theta_{max}$	17.8 / 38.6 deg
Boresight angle	θ_B	29.5°
Pulse and frontend parameters		
Guard time (after Tx window)	τ_{guard}	5 µs
Pulse (chirp) bandwidth	Bw_{chirp}	120 MHz
Antenna ohmic loss (two-way)	L_Ω	4.5 dB
System noise figure (temperature)	$F_n\ (T_n)$	3.5 dB (649 K)
Transmitted polarizations	-	V

Data rate related parameters		
Number of bits for Block-Adaptive Quantization (BAQ)	n_{bits}	4
Oversampling rate in range	γ_{rg}	1.265
Oversampling rate in azimuth	γ_{az}	1.200
SAR Performance requirements		
Two-dimensional resolution area (azimuth times ground range)	δ_{2D}	< 30 m^2
Noise Equivalent Sigma Zero	$NESZ$	< - 22 dB
Ambiguity-to-Signal Ratio (combination of range and azimuth ambiguities)	ASR	< - 23 dB

Table 1: Common simulation scenario parameters and SAR performance requirements for 350 km swath.

Antenna height in elevation	h_{el}	1.8 m
Antenna length in azimuth	l_{az}	12.0 m
Center frequency	f_0	5.4050 GHz
Number of Tx phase centers in elevation/azimuth (for analog beamforming)	M_{el}/M_{az}	40 / 1
Tx beamforming	-	Uniform taper in az. and Phase Spoiling in elev. (cf. **Figure 6**)
Number of Rx channels in elevation/azimuth	N_{el}/N_{az}	40 / 1
Channel spacing in elevation/azimuth	d_{el}/d_{az}	0.81 λ
Rx beamforming in elevation	-	SCORE with mode-dependent amplitude taper (Dolph-Chebyshev [21] with case-specific sidelobe parameters)

Table 2: Planar antenna parameters.

3.2 Operation in Staggered SAR mode

The Staggered SAR mode for this scenario, designed according to [15], is summarized in **Table 3**. As shown in **Figure 4**, the goal SAR performance is fulfilled with a mean PRF of 2250 Hz and average Tx power of 811 W. The inherent data rate of 3320 Mbps can be reduced to 1395 Mbps per polarization, which requires, however, on-board resampling [20].

Mean PRF	$\overline{PRF}$	2250.0 Hz
Number of PRIs	N_{PRI}	124 (5 sub-seqs.)
Initial PRI of each sub-sequence	PRI_0	[0.45, 0.46, 0.48, 0.49, 0.51] ms
Length of each sub-sequence	N_{sub}	[27, 25, 25, 24, 23]
PRI Step	Δ_{PRI}	-2.72 µs
PRI range	-	[375.99 - 509.38] µs
Processed bandwidth	BW_{proc}	788 Hz
Pulse duration (pulse duty cycle)	τ_P (dc)	22.2 µs (5.0 %)
Average Tx power	P_{avg}	811 W
Data rate wo. Doppler filtering	DR_{max}	3320 Mbps (SP) 6640 Mbps (DP)
Data rate with Doppler filtering	DR_{min}	1395 Mbps (SP) 2790 Mbps (DP)
Elevation Rx beamforming	-	SCORE (Cheb. Taper @ -30 dB)
Maximum number of simultaneous SCORE beams	N_{SCORE}	4

Table 3: Staggered SAR: Mode-specific parameters.

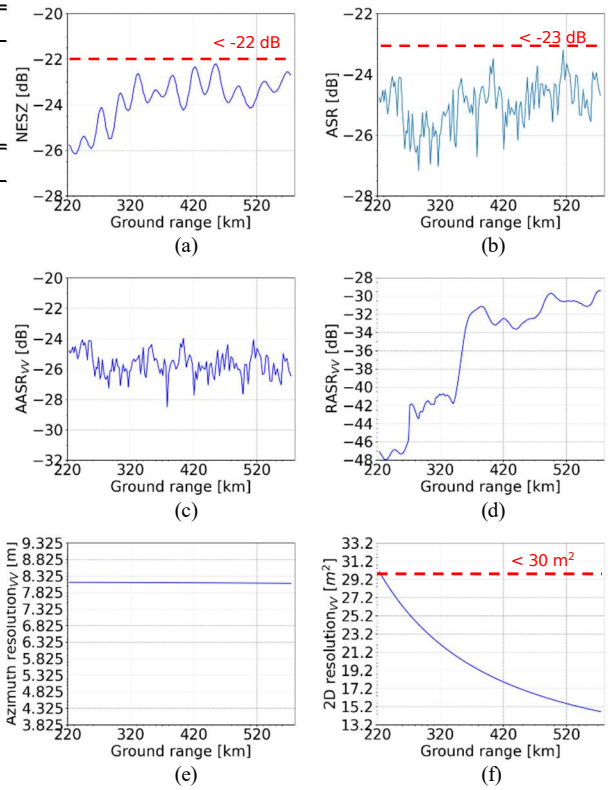

Figure 4: SAR Performance for the Staggered SAR mode. NESZ (a), ASR (b), AASR (c), RASR (d), Azimuth resolution (e) and 2D ground resolution (f) are shown. Imaging requirements are highlights by red dashed lines. A summary of the worst-case values is provided in **Table 5**.

3.3 Operation in Dual-PRI mode

A dual PRI mode is designed according to Section 2 to cover the same swath and fulfil the same SAR performance requirements. The $(N_1, N_2) = (2,3)$ configuration is chosen, as in **Figure 3**.

PRF (1st sequence)	PRF_1	1300.0 Hz
PRF (2nd sequence)	PRF_2	1950.0 Hz
Sequence relative length	(N_1, N_2)	(2, 3)
Delay between sequences	Δp	89.74 µs
PRIs of both sequences	$(PRI_1, PRI_2$	(769.23, 512.82) µs
Sequence "atom"	δ_A	256.4 µs
Processed bandwidth	BW_{proc}	773 Hz
Pulse duration (pulse duty cycle)	τ_P (dc)	38.5 µs (5.0 %)
Average Tx power	P_{avg}	1334 W: [841, 493] W
Data rate wo. Doppler filtering	DR_{max}	1941/4853 Mbps (SP) 3883/9707 Mbps (DP)
Data rate with Doppler filtering	DR_{min}	1385/3462 Mbps (SP) 2770/6924 Mbps (DP)
Rx beamforming in elevation	-	SCORE (Cheb. Taper @ -37 dB)
Maximum number of simultaneous SCORE beams	N_{SCORE}	5: 2 (1st seq.) + 3 (2nd seq.)

Table 4: Dual-sequence: Mode-specific parameters.

In this case, a $PRF_1 = 1300$ Hz is chosen, which causes Nadir returns to coincide with the co-blind ranges. Δp is chosen according to (8), given the PRF, the pulse duration and guard time provided in the table.

The timing is summarized in **Figure 5**, which shows that the coverage is indeed complementary between the two sequences and thus the design criterion is fulfilled. In the plot, the swath boundaries are indicated by vertical dashed lines. Pulses of the main sequence are shown in blue, whereas those of the secondary sequence are shown in red. These lead to co- and cross- blind ranges (denoted $Co - BR_n$ and $X - BR_k$ for orders n, k) with the colors of the sequence causing the gap. In the gaps, the solid color regions indicate range bins which are completely lost, whereas the transparent color regions are signals with reduced resolution, here treated as *blind ranges* without distinction. (Co-)Nadir returns are denoted N, whereas cross-Nadir returns are denoted $X - N_k$.

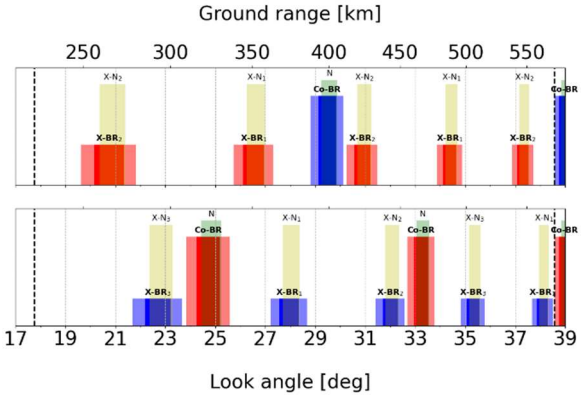

Figure 5: Timing of receiving windows in terms of ground range and look angle for the main sequence (top) and secondary one (bottom).

Complementary illumination for the second sequence is achieved by phase spoiling. The patterns for each sequence are seen in **Figure 6**. The same pattern as in the Staggered SAR case is used for the first sequence.

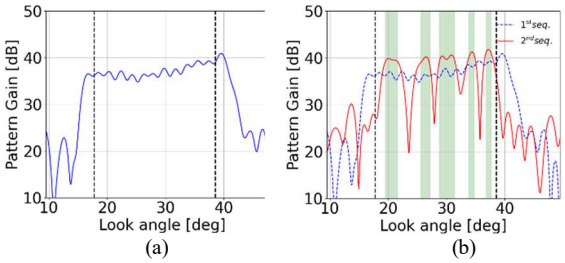

Figure 6: Elevation antenna patterns. Main elevation pattern (a) used for Staggered SAR and the first sequence of the dual-sequence mode. Pattern for second sequence (b) acquiring exclusivelly over the gaps of the first (highlighted by vertical green boxes). The swath boundaries are indicated by vertical dashed lines.

As seen in **Figure 7**, the SAR imaging requirements are fulfilled for the given parameters, requiring an average power of 1334 W (841 for the first and 493 for the second sequence), a 65% increase; but a reduced inherent (i.e. not requiring post-processing) data rate of 1941 Mpbs, a 42% reduction.

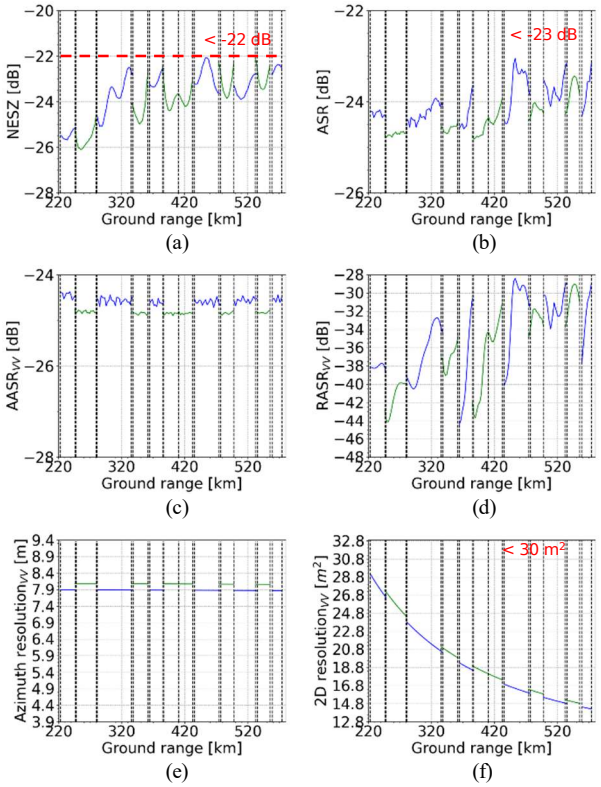

Figure 7: SAR Performance for the Dual-Sequence mode. (a) NESZ, (b) ASR, (c) AASR, (d) RASR, (e) Azimuth resolution and (f) 2D ground resolution are shown with the main sequence in blue and the secondary in green. Imaging requirements are highlights by red dashed lines. A summary of the worst-case values is provided in **Table 5**.

3.4 Performance Comparison

A comparison between the modes is provided in in **Table 5**.

Parameter / **Mode**	**Staggered SAR**	**Dual-Sequence**
(mean) PRF	2250 Hz	1300 Hz /1950 Hz
azimuth/	8.1 m /	8.2 m /
2D resolution	30.1 m²	29.2 m²
AASR	-24.0 dB	-24.4 dB
RASR	-29.4 dB	-28.4 dB
ASR	-23.2 dB	-23.0 dB
NESZ	-22.2 dB	-22.0 dB
Average Tx power	811 W	1334 W* [841, 493] W
SCORE taper	Chebyshev @ -30 dB	Chebyshev @ -37 dB
Data rate (per Rx polarization)	3320 Mbps	1941 Mbps
Data rate with Doppler filtering	1395 Mbps	1385 Mbps

*This value is the sum for both sequences, the power per sequence (main, secondary) is also provided.

Table 5: Worst-case SAR performance and mode parameters comparison.

The performance is fulfilled with a lower sampling rate than staggered SAR, but a higher average Tx power (note the power for on-board processing is not accounted for). This is due to the fact that additional pulses are transmitted and practical limits exist to the degree of complementarity of the illumination in **Figure 2**, meaning some degree of redundant illumination cannot be avoided and the Tx power will thus increase by a factor within the range 1 (ideal, no redundancy) to 2 (complete redundancy).

Staggered SAR shows the advantage of flexible coverage (arbitrary range and PRF combinations are possible), at the price of higher data rates, which drive up on-board complexity. The smearing of the ambiguities [22] can also be seen as an advantage. The new Dual-Sequence Stripmap mode in turn presents itself as a feasible option to avoid high data rates and limit on-board complexity, provided that average power is not a major constraint in the observation scenario.

4 Conclusion

The paper discusses a new Dual-Sequence Stripmap mode in which the problem of blind ranges in a very wide swath SAR acquisition is dealt with by transmitting two interleaved constant-PRI sequences and mosaicking the images (formed independently) from the two. The main motivation is to obtain a Doppler-gap free acquisition with reduced data rate and thus save on on-board system complexity. This mode belongs to the class of multiple elevation beam (multi SCORE) modes with digital beamforming in elevation. A timing analysis and a design criterion for the mode were examined.

The imaging scenario showed the feasibility of achieving high levels of SAR performance in this mode, with a data rate similar to conventional Stripmap, as long as the pulse duty cycles are relatively short (in the example around 5%) and the second sequence images exclusively the gaps of the first one. The interleaving of the pulses has two disadvantages. First, reduced pulse proximity drives up the range ambiguities. This indicates the mode requires a suitably high antenna in elevation (which is however expected for SCORE systems) and adequate digital beamforming on receive. A lower PRF is thus also clearly beneficial. Second, transmitting more pulses requires more power, as the effective pulse duty cycle is increased. This disadvantage is to some extent mitigated by the reduced power consumption of the on-board electronics, in case of no or very simple on-board processing.

References

[1] J. Curlander, R. McDonough: *Synthetic Aperture Radar: Systems and Signal Processing*, Jon Wiley & Sons, 1991.

[2] K. Tomiyasu: *Conceptual performance of a satellite borne wide swath synthetic aperture radar*, in IEEE Trans. Geosci. Remote Sens., vol. GRS-19, no. 2, pp. 108-116, April 1981.

[3] R. K. Moore, J. P. Claassen and Y. H. Lin: *A scanning spaceborne synthetic aperture radar with integrated radiometer*, in IEEE Trans. Aerosp. Electron. Syst., vol. AES-17, no. 3, pp. 410-421, May 1981.

[4] A. Currie, M. A. Brown: *Wide-swath SAR*, in IEE Proceedings F - Radar and Signal Processing, vol. 139, pp. 122-135, 1992.

[5] G. Callaghan, I. Longstaff: *Wide-swath spaceborne SAR using a quad-element array,* in IEE Proc. RSN, vol. 146, pp. 159-165, 1999.

[6] G. Krieger, N. Gebert, and A. Moreira: *Multidimensional waveform encoding: A new digital beamforming technique for synthetic aperture radar remote sensing,* in IEEE Trans. Geosci. Remote Sens., vol. 46, no. 1, pp. 31–46, January 2008.

[7] N. Gebert, G. Krieger and A. Moreira, "Multichannel Azimuth Processing in ScanSAR and TOPS Mode Operation," in *IEEE Transactions on Geoscience and Remote Sensing*, vol. 48, no. 7, pp. 2994-3008, July 2010.

[8] M. Bartusch, C. Bruens, S. Stettner and A. Nuncio Quiroz, "HRWS: The upcoming German X-Band Spaceborne SAR Mission," in *13th European Conference on SAR (EUSAR 2021)*, pp. 1-4, Dresden (online event), Germany, 2021.

[9] M. Suess, B. Grafmueller, R. Zahn: *A novel high resolution, wide swath SAR system*, in Proc. IGARSS, Sydney, 2001.

[10] G. Krieger, *et al.*: *Advanced Concepts for Ultra-Wide-Swath SAR Imaging*, in 7th European Conference on Synthetic Aperture Radar (EUSAR 2008), pp. 1-4, Friedrichshafen, Germany, 2008.

[11] G. Krieger *et al.*: *SIMO and MIMO System Architectures and Modes for High-Resolution Ultra-Wide-Swath SAR Imaging*, in 11th European Conference of Synthetic Aperture Radar (EUSAR*)*, pp. 1-6., Hamburg, 2016.

[12] M. Younis *et al.*, *Techniques and Modes for Multi-Channel SAR Instruments*, in 11th European Conference of Synthetic Aperture Radar (EUSAR), pp. 1-6., Hamburg, 2016.

[13] M. Suess and W. Wiesbeck: Side-looking synthetic aperture radar system, European Patent EP 1 241487, Sept., 2002.

[14] N. Gebert, G. Krieger and A. Moreira: *Digital Beamforming on Receive: Techniques and Optimization Strategies for High-Resolution Wide-Swath SAR Imaging*, in IEEE Trans. Aerosp. Electron. Syst., vol. 45, no. 2, pp. 564-592, 2009.

[15] M. Villano, G. Krieger and A. Moreira: *Staggered SAR: High-Resolution Wide-Swath Imaging by Continuous PRI Variation*, in IEEE Trans. Geosci. Remote Sens., vol. 52, no.7, pp.4462-4479, 2014.

[16] F. Queiroz de Almeida, M. Younis, G. Krieger and A. Moreira: *On a Dual PRI Pulse Sequence Mode for High-Resolution Wide-Swath SAR Imaging* in Proc. IGARSS, Brussels, 2021.

[17] M . Younis, G. Krieger and A. Moreira: *On a Dual PRI Pulse Sequence Mode for High-Resolution Wide-Swath SAR Imaging* in Proc. IGARSS, Brussels, 2021.

[18] G. Di Martino and A. Iodice, "Coprime Synthetic Aperture Radar (CopSAR): A New Acquisition Mode for Maritime Surveillance," in *IEEE Transactions on Geoscience and Remote Sensing*, vol. 53, no. 6, pp. 3110-3123, June 2015.

[19] P. Potin *et al.*, "Sentinel-1 Constellation Mission Operations Status," *IGARSS 2018 - 2018 IEEE International Geoscience and Remote Sensing Symposium*, 2018, pp. 1547-1550.

[20] M. Villano, G. Krieger and A. Moreira, "Onboard Processing for Data Volume Reduction in High-Resolution Wide-Swath SAR," in *IEEE Geoscience and Remote Sensing Letters*, vol. 13, no. 8, pp. 1173-1177, Aug. 2016.

[21] H. L. V. Trees, *Optimum Array Processing*, New York: John Wiley & Sons Inc., 2002.

[22] M. Villano, G. Krieger and A. Moreira "Ambiguities and image quality in staggered SAR*"* in *5th Asia-Pacific Conference on Synthetic Aperture Radar (APSAR),* Singapore, pp. 204-209*,* 2015.